Title

S-Nitrosylation-mediated dysfunction of TCA cycle enzymes in synucleinopathy studied in postmortem human brains and hiPSC-derived neurons

Journal

Cell Chemical Biology, 30(8)

ISSN

2451-9456

Authors

Doulias, Paschalis-Thomas

Yang, Hongmei

Andreyev, Alexander Y

et al.

Publication Date

2023-08-01

DOI

10.1016/j.chembiol.2023.06.018

Peer reviewed

HHS Public Access

Author manuscript

Cell Chem Biol. Author manuscript; available in PMC 2024 August 17.

Published in final edited form as:

Cell Chem Biol. 2023 August 17; 30(8): 965–975.e6. doi:10.1016/j.chembiol.2023.06.018.

S-Nitrosylation-mediated dysfunction of TCA cycle enzymes in synucleinopathy studied in postmortem human brains and hiPSC-derived neurons

Paschalis-Thomas Doulias[1,2,7], **Hongmei Yang**[3,4,7], **Aleksander Andreyev**[5,7], **Nima Dolatabadi**[5,7], **Henry Scott**[5], **Charlene K Raspur**[5], **Parth R. Patel**[5], **Tomohiro Nakamura**[5], **Steven R. Tannenbaum**[3], **Harry Ischiropoulos**[1], **Stuart A. Lipton**[5,6,8,*]

[1]Children's Hospital of Philadelphia Departments of Pediatrics and Pharmacology, Perelman School of Medicine, University of Pennsylvania, Philadelphia, Pennsylvania 19104, USA

[2]Department of Chemistry, University Research Center of Ioannina, University of Ioannina 45110, Greece

[3]Department of Biological Engineering, Massachusetts Institute of Technology, Cambridge, MA 02139, USA

[4]Changchun University of Chinese Medicine, Changchun 130021, China

[5]Neurodegeneration New Medicines Center, The Scripps Research Institute, La Jolla, CA 92037, USA

[6]Department of Neurosciences, University of California, San Diego, School of Medicine, La Jolla CA 92093, USA

[7]These authors contributed equally

[8]Lead contact

SUMMARY

A causal relationship between mitochondrial metabolic dysfunction and neurodegeneration has been implicated in synucleinopathies, including Parkinson's disease (PD) and Lewy body dementia (LBD), but underlying mechanisms are not fully understood. Here, using human induced pluripotent stem cell (hiPSC)-derived neurons with mutation in the gene encoding α-synuclein (αSyn), we report the presence of aberrantly S-nitrosylated proteins, including tricarboxylic acid (TCA) cycle enzymes, resulting in activity inhibition assessed by carbon-labeled

*Correspondence: slipton@scripps.edu.

AUTHOR CONTRIBUTIONS

Conceptualization, S.A.L.; methodology, P.-T.D., H. Y., N.D., A.A., S.R.T., H.I., and S.A.L.; investigation, P.-T.D., H. Y., N.D., P.R.P., C.K.R., and T.N.; visualization, P.-T.D., H. Y., N.D., A.A., H.S., and T.N.; funding acquisition, T.N., S.R.T., H.I., and S.A.L..; writing – original draft, S.A.L.; writing – review & editing, P.-T.D., H. Y., N.D., A.A., T.N., S.R.T., H.I., and S.A.L.

DECLARATION OF INTERESTS

The authors declare no competing interests.

metabolic flux experiments. This inhibition principally affects α-ketoglutarate dehydrogenase/ succinyl coenzyme-A synthetase, metabolizing α-ketoglutarate to succinate. Notably, human LBD brain manifests a similar pattern of aberrantly S-nitrosylated TCA enzymes, indicating the pathophysiological relevance of these results. Inhibition of mitochondrial energy metabolism in neurons is known to compromise dendritic length and synaptic integrity, eventually leading to neuronal cell death. Our evidence indicates that aberrant S-nitrosylation of TCA cycle enzymes contributes to this bioenergetic failure.

eTOC Blurb

Mitochondrial metabolic dysfunction and generation of excessive NO/RNS are thought to contribute to synucleinopathies. Here, Doulias and colleagues reveal that aberrant protein S-nitrosylation of TCA cycle enzymes, especially αKGDH, leads to inhibition in flux through the TCA cycle, contributing to neurodegenerative phenotypes in models of synucleinopathies.

Graphical Abstract

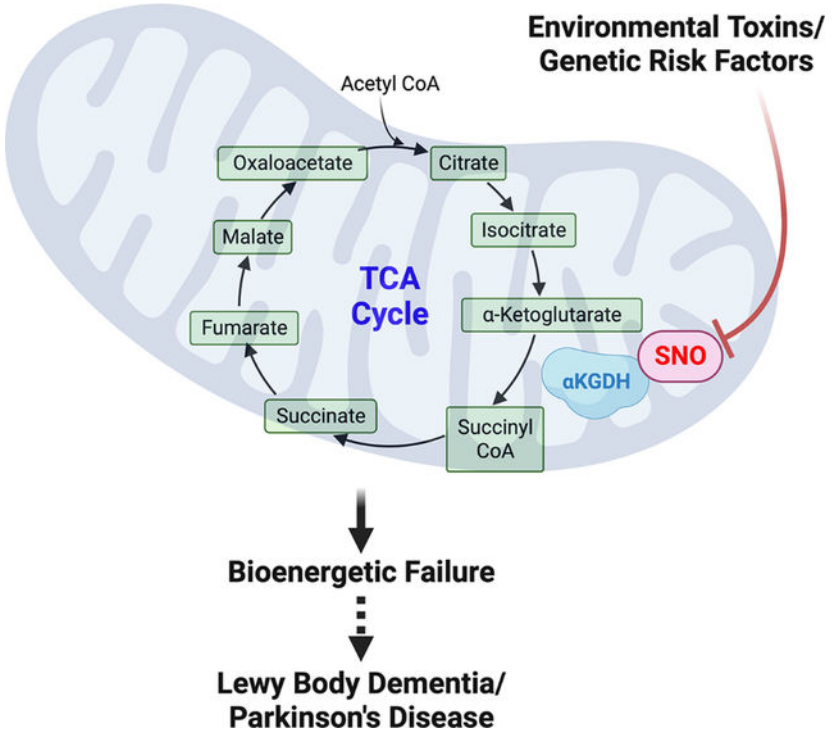

INTRODUCTION

Mitochondrial deficits are thought to contribute to neurodegenerative disorders, including synucleinopathieslike PD and LBD.[1,2] Mitochondrial-based energy deficits have been identified in synucleinopathies in human brain and animal models, and in human PD patient induced pluripotent stem cell (hiPSC)-derived A9-type dopaminergic neurons (abbreviated hiN), the initial cell type lost in PD; this energy compromise likely contributes to dendritic damage, synaptic loss, and eventually neuronal cell death.[3–8] Moreover, PET

scans in human LBD patients reveal hypometabolism in several brain regions.[9] In this regard, dysfunction of the mitochondrial TCA cycle involving multiple enzymes has been identified in several neurodegenerative disorders including PD and LBD.[10] Nonetheless, the underlying mechanism(s) for TCA cycle dysfunction and the full extent of the energy compromise remain unknown. Here, we used hiPSCs to model PD/LBD and report the presence of aberrant S-nitrosylation of many proteins, including TCA cycle enzymes, which inhibits the activity of these enzymes.[11] Using ^{13}C dynamic labeling, we observed specific changes in central carbon metabolism indicating defects in the TCA cycle that correlate to the enzymes manifesting aberrant S-nitrosylation.

We also compared the S-nitrosylation pattern of TCA enzymes in human postmortem brains with synucleinopathy to that found in the hiPSC-based model of PD/LBD. For this purpose, we studied hiN bearing an A53T point mutation in the gene *SNCA* encoding α-synuclein (αSyn) protein, which is known to result in PD/LBD, versus isogenic, gene-corrected controls. We found remarkable concordance of results in the S-nitrosylation pattern of TCA enzymes in human brain synucleinopathy and in A53T-hiN. These findings gave us added confidence that our hiPSC-based model system manifested pathophysiologically-relevant changes in enzyme S-nitrosylation and thus inhibition of TCA cycle function.

Prior work had revealed mitochondrial defects in A53T mutant hiN compared to isogenic controls, in part mediated by nitric oxide (NO)-related species generated in response to mutant aggregated αSyn as well as to pesticide exposure.[4,5,8,12] Mitochondrial dysfunction was demonstrated as a compromise in maximal respiratory capacity assessed with the Seahorse extracellular flux analyzer platform, whereas basal glycolytic capacity, monitored by extracellular acidification rate (ECAR), was little affected.[5] We had previously found that the A53T mutant hiN generate excessive reactive oxygen species (ROS) compared to isogenic controls, but reactive nitrogen species (RNS) were even more predominant and destructive, as evidenced by protection of neurons by the NO synthase inhibitor L-N^G-Nitro arginine methyl ester (L-NAME).[5] Mechanistically, NO has been shown to react with cytochrome C in the electron transport chain (ETC) to inhibit oxygen consumption rate. Moreover, at low concentrations, NO can compete with O_2 for binding to the terminal complex of the ETC, among other NO reactions on the ETC.[13–25] Here, to determine if dysfunction in the TCA cycle might also underlie, at least in part, these mitochondrial and bioenergetic defects, we performed metabolic flux experiments with isotopically-labeled carbon substrate to trace the metabolism of the labeled carbon atoms through the TCA cycle in PD patient hiN vs. isogenic WT/Controls.

RESULTS

Defects in TCA cycle function in A53T-hiN as assessed by metabolic flux

In contrast to neuronal stem cells, which primarily use glucose metabolized by glycolysis for their energy supply,[26] it is widely thought that basal neuronal energy in the mature brain is generated by the TCA cycle after influx of lactate, supplied by astrocytes, into neurons (termed astrocyte-neuron lactate shuttle [ANLS]).[27–29] In this scenario, astrocytes generate lactate via glycolysis and export lactate to neurons for conversion into pyruvate, feeding into the TCA cycle, which appears to be critical for neuronal health and function under

basal conditions. Notably, during periods of intense stimulation, neurons may be capable of using glucose directly.[30] Nonetheless, since PD and LBD are chronic diseases, it seemed appropriate initially to test long-term energy requirements by assessing the ANLS system, as such energy is critical for normal synaptic function.[31,32] In fact, recent evidence suggests that lactate is the major source of energy underlying cognition affected in PD/LBD and other dementias.[33] This aim was accomplished by supplying isotopically labeled lactate to neurons for metabolic analysis. Accordingly, we performed metabolic flux experiments after supplying C^{13}-lactate as the sole source of energy to hiN cultures, comparing the results of A53T mutant to isogenic, gene-corrected controls (labeled as "Corrected" in figures). Importantly, the use of isogenic controls minimized the potential obfuscating effect of genetic background.[5,34]

For these metabolic experiments, hiN were grown in two-dimensional cultures without astrocytes to which labeled lactate was added (in order to simulate lactate supplied by astrocytes to neurons). Lactate is taken up by the neurons and then converted to pyruvate to supply the TCA cycle, whose individual enzyme activities (flux through the system) could be monitored via metabolic flux of labeled metabolites (Figure 1 and Figure S1), as described previously.[35–37] To interpret these data, the following principles were employed:[38]

1. Inhibition of a particular enzyme results in increased ^{13}C-labeled substrate and decreased ^{13}C-labeled product, producing an increased substrate/product ratio, as measured from lysates by liquid chromatography-mass spectrometry (LC-MS) of TCA metabolites.

2. Relief of enzyme inhibition results in a decrease in the ratio back towards baseline. To achieve this, we used the NO synthase inhibitor, L-NAME. This was based on prior work[5] showing that a fall in oxygen consumption rate (reflecting decreased ATP production by mitochondria) was associated with excessive generation of NO/RNS in A53T-hiN. This increase in NO/RNS was strikingly more apparent in A53T-hiN after exposure to the herbicide/fungicide combination of paraquat (PQ) and maneb (MB),[5] known to inhibit the ETC and to be associated with PD pathogenesis. The relevance of PQ/MB further increasing NO/RNS generation in the face of a genetic mutation such as A53T highlights the importance of gene x environment (GxE) effects in the pathogenesis of PD.[5] Blocking the generation of RNS with L-NAME should prevent aberrant protein S-nitrosylation at critical cysteine residues that has been shown to occur in or near active sites of multiple enzymes that would affect metabolic flux through the TCA cycle.[11,39] Additionally, the converse is also true – exposure to an NO donor/transnitrosylating agent such as S-nitrosocysteine (SNOC) would increase protein S-nitrosylation of TCA enzymes.[11,39] Note, however, that L-NAME itself can produce very low, chronic levels of NO,[40] which can become more apparent at low basal levels of NOS activity when little endogenous NO is produced.

3. For C^{13}-lactate supplying the TCA cycle, the first two ^{13}C-labeled carbons in the TCA enzyme substrates and products (labeled M+2) are likely to be supplied to the TCA cycle directly by lactate via one turn through the cycle; whereas,

if additional carbons are considered they may come from ancillary pathway metabolism (Figure S1).[35–37,41–44] Hence, the figures shown here present raw data (after correction for background atmospheric C^{13} and normalization for mass); this is labeled M+2 ME (molar enrichment) for each substrate and product (Figure 1, *left-hand panels*). Additionally, the ratio of substrate/product is shown, labeled M+2 MER (Figure 1, *right-hand panels*). Total ME and MER data for each pair of metabolites is shown in Figures S2 and S3.

Inhibition of metabolic flux at the level of aconitase and isocitrate dehydrogenase

As judged from the citrate (Cit) to α-ketoglutarate (αKG) ratio (Figure 1A), the interpretation of the metabolic flux experiments is most consistent with little if any effect at the level of aconitase/isocitrate dehydrogenase (AC/IDH) on isogenic WT/Corrected neurons in the presence or absence of PQ/MB pesticides. Changes were evident, however, in the A53T αSyn hiN compared to WT/Corrected, with increases in the Cit/αKG ratio ($p \leq 0.04$ by ANOVA) particularly in the presence of PQ/MB ($p \leq 0.04$) or SNOC ($p \leq 0.0007$) (Figure 1A, *right-hand panel*). These changes are consistent with aconitase being inhibited and IDH impacted under these conditions.

There was a trend for L-NAME to increase the Cit/αKG ratio but it did not reach significance. Such changes could result from L-NAME-mediated relief from a larger downstream block due to S-nitrosylation in the TCA cycle, as shown below. Notably, in the A53T αSyn compared to WT/Corrected hiN, L-NAME significantly increased Cit levels ($p \leq 0.02$, Figure 1A, *left-hand panel*). A contributory factor for this effect is that pyruvate dehydrogenase (E1 subunit) may be partially inhibited due to S-nitrosylation (see below). In that case, L-NAME would relieve that block, thus increasing citrate (see schematic in Figure 2). This would be expected to be even more evident with higher levels of NO/RNS, as was the case for the A53T-PQ/MB condition (increased citrate, $p \leq 0.015$, Figure 1A, *left-hand panel*) and increased Cit/αKG ratio ($p \leq 0.0006$, Figure 1A, *right-hand panel*). Interestingly, under these conditions, αKG also fell ($p \leq 0.03$, Figure 1A, *left-hand panel*), indicating that flux through a subsequent step in response to L-NAME also occurred as S-nitrosylation was reversed.

Inhibition of metabolic flux at the level of α-ketoglutarate dehydrogenase/succinyl coenzyme-A synthetase

At the next steps in the TCA cycle, i.e., at the level of α-ketoglutarate dehydrogenase/ succinyl coenzyme-A synthetase (αKGDH/SCS), as reflected in the αKG/succinate (Succ) ratio (Figures 1B and 2), the effect of A53T compared to WT/Corrected became apparent in the presence of PQ/MB ($p \leq 0.04$, Figure 1B), *right-hand panel*). Increased αKG ($p \leq 0.02$, Figure 1B, *left-hand panel*) in A53T compared to WT/Corrected with an overall increase in the αKG/Succ ratio in the presence of PQ/MB ($p \leq 0.02$, Figure 1B, *right-hand panel*), or after exposure to SNOC in WT/Corrected ($p \leq 0.03$, Figure, 1B, *right-hand panel*), may reflect a relative block at the level of αKGDH/SCS, induced by NO-related species. With the addition of L-NAME, however, the ratio of a αKG/Succ increased in WT/Corrected neurons even without exposure to PQ/MB ($p \leq 0.04$, Figure, 1B, *right-hand panel*), but decreased in A53T neurons, especially when compared in the presence and absence PQ/MB

($p \leq 0.01$, Figure, 1B, *right-hand panel*). The latter reflects L-NAME relief of inhibition from S-nitrosylation at the level of αKGDH/SCS since A53T-hiNs are known to have much more NO production from NOS than WT/Corrected neurons, especially in the presence of PQ/MB, as shown in Figure 4 of Ryan et al.[5] In contrast, in WT/Corrected hiNs with low basal levels of NOS activity at baseline, which cannot be inhibited below baseline by L-NAME, the production of very small levels of NO by L-NAME itself would result in increased protein S-nitrosylation and hence some degree of inhibition of αKGDH/SCS enzymatic activity compared to basal activity as observed.

Lack of inhibition of metabolic flux at the level of succinate dehydrogenase

At the level of succinate dehydrogenase (SDH, Figures 1C and 2), as reflected in the succinate/fumarate (Succ/Fum) ratio for WT/Corrected, A53T ($p \leq 0.03$) or A53T-PQ/MB ($p \leq 0.03$) slightly decreased the ratio, while L-NAME reversed this effect for A53T-PQ/MB ($p \leq 0.015$) (Figure 1C, *right-hand panel*). These results are mostly opposite of the changes seen with Cit/αKG and reflect a downstream block in TCA cycle enzyme activity by S-nitrosylation as evidenced, for example, by the uniform increase in Succ ($p \leq 0.015$) and Fum ($p \leq 0.002$) levels in the A53T neurons compared to their WT/Corrected counterparts (Figure 1C, *left-hand panel*).

Minor inhibition of metabolic flux at the level of malate dehydrogenase

Distally in the TCA cycle, at the level of malate dehydrogenase (MDH), compared to WT/Corrected, we observed a slight increase in the ratio of malate to oxaloacetate (Mal/OAA) for A53T-PQ/MB and for the combination of A53T plus SNOC exposure ($p \leq 0.2$, Figures 1D, *right-hand panel*, and 2). This was reflected mainly as increased labeled malate ($p \leq 0.002$, WT/Corrected compared to all A53T values unless L-NAME was present, Figure 1D, *left-hand panel*). While these data indicate a relative block at this level, a further increase in the Mal/OAA ratio occurred with the addition of L-NAME (e.g., for A53T-PQ/MB, $p \leq 0.03$). This fact, coupled with the finding that both Mal ($p \leq 0.002$) and OAA ($p \leq 0.0007$) increased in the A53T neurons compared to WT/Corrected (Figure 1D, *left-hand panel*), is explained by more prominent block elsewhere in the TCA cycle that is relieved by NOS inhibition, as we have shown occurs at the level of αKGDH/SCS where L-NAME reversed the block in metabolic flux (Figure 1B).

In summary, the inhibition of metabolic flux at the level of αKDGH/SCS was consistently reversed by L-NAME, suggesting that this was the site of the most significant block in the TCA cycle in A53T-hiN by S-nitrosylation, particularly in the presence of PQ/MB, with more minor inhibitory effects mediated at the level of AC/IDH and MDH. Kinetic modeling corroborated these results (see Figure 2). Quantitatively, using kinetic modeling (see METHOD DETAILS), we found decreases in rate constants for the A53T-PQ/MB condition compared to WT/Corrected for the enzymatic steps at CS/PDH, AC/IDH, αKDGH/SCS, and FH. Notably, however, only the rate constant for αKDGH/SCS increased significantly (4-fold, $p < 0.001$ by ANOVA) for A53T-PQ/MB values after addition of L-NAME, indicating relief of inhibition and consistent with the notion that this was the major site of blockade in the TCA cycle by S-nitrosylation. Thus, the kinetic rate constants yielded results in accord

with the major effect of aberrant S-nitrosylation occurring at the αKDGH/SCS step in our PD/LBD hiPSC model system.

Protein S-nitrosylation of TCA enzymes in A53T-hiN

To test our hypothesis that alterations in TCA cycle activity in A53T vs. isogenic control hiN were due to aberrant protein S-nitrosylation, we performed MS-based analysis of the S-nitroso(SNO-)proteome in hiN after enrichment for SNO-peptides with an organomercury affinity column enrichment, as previously described,[45,46] under all six conditions tested here (Vehicle-treated Corrected (isogenic control), Vehicle-treated A53T, Corrected PQ/MB, A53T PQ/MB, Corrected SNOC, and A53T SNOC). The key data are summarized in a Venn diagram analysis in Figure 3A, and the entire SNO-proteome dataset is presented in Table S1. In Vehicle-treated Corrected hiN, 59 proteins were endogenously S-nitrosylated in our samples. In contrast, in A53T-hiN and A53T-hiN exposed to PQ/MB, 81 and 203 SNO-proteins were encountered, respectively. As a positive control, in an effort to maximize the potential number of S-nitrosylation sites, we exposed Corrected hiN and A53T-hiN to SNOC. Under these conditions, the two groups displayed approximately the same number of SNO-proteins (253 and 244, respectively). The major differences germane to our findings were observed in the Vehicle-treated Corrected vs. A53T + PQ/MB (Figure 3A). A Gene Ontology (GO)-term analysis of these differences revealed that the highest scoring pathways all involved metabolism, with carbohydrate metabolism and the TCA cycle high on the list.

Moreover, we found virtually perfect concordance between S-nitrosylated TCA cycle enzymes predicted from the metabolic flux experiments (Table S1 and Figure 2), and thus inhibited.[11,47] Specifically, with our MS technique, we found evidence for S-nitrosylation of mitochondrial AC/IDH in A53T-hiN in the presence of PQ/MB, and in Corrected or A53T-hiN after SNOC exposure. As a second confirmatory assay, the biotin-switch method confirmed the presence of SNO-AC in the A53T-hiN cells (Figure S4). These represent the very same conditions in which we observed inhibition in the metabolic flux experiments at the level of AC/IDH (Figure 1A).

At the next step in the TCA cycle, αKGDH/SCS (also known as 2-oxoglutarate dehydrogenase and succinyl CoA ligase, respectively, in Table S1), with our MS technique, we again observed S-nitrosylation of A53T-hiN in the presence of PQ/MB, and in Corrected or A53T-hiN after SNOC exposure. Note that for αKGDH the E3 subunit (designated dihydrolipoyl dehydrogenase, DLD) was S-nitrosylated. As a confirmatory assay, the biotin-switch method confirmed the presence of SNO-DLD in the A53T-hiN cells (Figure S4). We have previously shown that formation of SNO-DLD at levels similar to those found here (as judged by the ratio of S-nitrosylated DLD to total DLD (Figure S4C) profoundly inhibits its activity.[11] This finding is in perfect register with the conditions that caused inhibition of metabolic flux at this level in the TCA cycle.

The next step in the TCA cycle, SDH, also represents complex II in the ETC, as shown in the schema in Figure 2. Our metabolic flux experiments predicted no inhibition at this level of the TCA cycle/ETC, and indeed no S-nitrosylation of SDH was observed under any of the conditions in Corrected WT or A53T-hiN.

Finally, for mitochondrial MDH (MDH2 in Table S1), we found S-nitrosylation in A53T-hiN in the presence of PQ/MB, and in Corrected or A53T-hiN after SNOC exposure. These results are in accord with our findings of some degree of inhibition in metabolic flux at this step exclusively in A53T-hiN exposed to PQ/MB or SNOC. Note also that cytoplasmic MDH (MDH1 in Table S1) is S-nitrosylated under these conditions, consistent with the notion that the alternative anaplerotic pathway access of malate or OAA into the TCA cycle would also be inhibited. Additionally, in A53T-hiN exposed to PQ/MB, pyruvate dehydrogenase (PDHA1, E1 component, subunit α, as well as DLD, which is also the E3 component of PDH as it is for αKGDH) was also S-nitrosylated (Table S1), consistent with our observation that L-NAME relieved inhibition at this site, thus increasing labeled citrate in the metabolic flux experiments (Figure 1A, *left-hand panel*). Thus, for each of the S-nitrosylation events in TCA cycle enzymes the findings are consistent with the notion that this posttranslational modification is responsible for the observed inhibition in metabolic flux observed there.

Protein S-nitrosylation of TCA and related enzymes in human LBD brain

To assess the pathophysiological relevance of our findings in cultured A53T-hiN, we next assessed the S-nitrosoproteome of brains with short postmortem times (less than 6 hours) for LBD and control human patients (Table S2). Using the *SNO*TRAP technique that we have previously described for assessment of the SNO-proteome in whole brain, we found in LBD and control brains a total of 943 S-nitrosylated proteins at 1552 SNO-sites on the proteome, with 196 SNO-proteins exclusively in LBD brain and 176 exclusively found in control brains (Figure 4A–D). In these samples all cell types in brain are assessed, so the data are not strictly comparable to the pure neuronal cultures of the A53T-hiN samples. Nonetheless, we observed a significant enrichment for S-nitrosylated proteins associated with the TCA cycle in LBD brains over controls (Tables S3 and S4). In fact, reactome pathway analysis with STRING software showed that the TCA cycle and ETC were the second most represented pathway affected by protein S-nitrosylation (Figure 4E). Notably, among the S-nitrosylated TCA enzymes in LBD brains compared to controls, αKGDH was the most significantly elevated (Figure 4D, Tables S3 and S4). This result is consistent with our findings in the A53T-hiN S-nitrosoproteome and for the step in the TCA cycle most inhibited in the metabolic flux experiments.

DISCUSSION

We describe partial inhibition TCA cycle flux in A53T-hiN caused by aberrant protein S-nitrosylation of several enzymes, most prominently at the αKGDH step, which would normally produce NADH and convert αKG to succinate. NADH is thus supplied to complex I of the ETC, and succinate as substrate to SDH, which also functions as complex II of the ETC (Figure 2). Therefore, inhibition of αKGDH results in both a decrease in substrate for SDH/complex II and also prevents NADH supply to complex I, thus limiting the production of ATP by mitochondria.[5,39,41,43,44,48] In this manner, formation of SNO-αKGDH would contribute to the severe bioenergetic compromise observed in A53T-hiN.[5] Collectively, in both animal models and in hiPSC-based models, we and others have causally linked such bioenergetic compromise in mitochondria to the pathogenesis of PD and LBD by

contributing to neurite and synaptic loss, and eventually to neuronal cell death.[3,5–7,10] The present study links these findings of compromised mitochondrial bioenergetics to TCA cycle compromise, precipitated by aberrant protein S-nitrosylation reactions of TCA cycle enzymes in PD/LBD brain.

Along these lines, our prior studies had demonstrated generation of excessive NO/RNS, and aberrant protein S-nitrosylation in A53T-hiN.[5] The idea here is that a genotype makes the cells more susceptible to environmental influences, e.g., pesticides, which are known to be associated with PD/LBD, as we had shown previously.[5] Note, however, that in the context of various genetic backgrounds, environmental toxins alone may be able to exert profound deleterious effects. One of the major GxE interactors is NO production, which is synergistically enhanced by the presence of both an A53T αSyn mutation and exposure to pesticides such as PQ/MB.[5] In the present study, we show how these elevated levels of NO affect metabolism via TCA cycle inhibition. From epidemiological studies in a real-world scenario, we know that both genotype and pesticides increase NO production contributing to nitrosative stress and PD risk.[5] Hence, in the case of SNO-proteins, genotype and pesticides work in concert as an example of GxE interaction. We show here for the first time a link between aberrant protein S-nitrosylation and TCA cycle enzyme inhibition to potentially contribute to PD/LBD pathogenesis.

Moreover, we recently showed that S-nitrosylation at critical Cys residues of several TCA cycle enzymes inhibits their catalytic activity.[11] With this background, we present evidence for aberrant protein S-nitrosylation of multiple TCA cycle enzymes in A53T-hiN, which leads to TCA cycle dysfunction. The predominant site of blockade appears to be at αKGDH/SCS based on metabolic flux analysis with inhibition at this step that is reversed by the NOS inhibitor L-NAME; more minor blocks occur at the AC/IDH and MDH steps. In accordance with this conclusion, we found that αKGDH is aberrantly S-nitrosylated to a degree (Figure S4) that we have previously shown inhibits its enzymatic activity, as judged by the relative ratio of S-nitrosylated subunit to total subunit protein.[11] Thus, this aberrant S-nitrosylation may account for the principal block at the level of αKGDH. Notably, analysis of the S-nitrosoproteome of postmortem human LBD brain revealed that among the S-nitrosylated TCA enzymes, αKGDH was the most heavily S-nitrosylated (Table S3), providing pathophysiological relevance for our similar findings in cultured A53T-hiNs. Since approximately half of the cells in the human cerebrocortex are glia and half neurons,[49] and we are assaying aberrant neuronal SNO-TCA enzymes in the hiN model studied here, we might expect that approximately half as much enzyme (e.g., as reflected in the relative ratio of SNO-DLD/total DLD, representing the E3 subunit of αKGDH) would be S-nitrosylated in diseased postmortem brain as in hiN, and this is indeed what we observed in human LBD brain compared to control (viz. Table S3 and Figure S4).[50–52] The S-nitrosylation-induced TCA cycle inhibition demonstrated here in all likelihood contributes to the mitochondrial bioenergetic compromise previously shown to be associated with nitrosative stress in these cells,[5] and thus to dendritic/synaptic damage and eventual neuronal cell death linked to mitochondrial respiratory failure.[3,5–7,10,51–54] Additionally, these results may also have implications for the treatment of synucleinopathies because rescue of the energy supply may preserve neuronal form and function.[3,39,55]

Limitations of the study

Studies using cultured neurons represent *in vitro* conditions, whether in 2D or 3D cultures,[56] and thus that inform on what is plausible but do not faithfully replicate *in vivo* conditions. In our case, pure hiN in the absence of astrocytes could be viewed as an artificial system. That said, this approach allows the assessment of human cells from a patient with the disease process. Moreover, comparison to isogenic, gene-corrected controls allows contextual comparison in the same genetic background. The fact that several features of synucleinopathy are faithfully reproduced in these A53T-hiN cultures[5,6] gave us increased confidence that aspects of PD/LBD could be reproduced and studied. For example, the mitochondrial deficits, presence of aberrantly S-nitrosylated proteins, αSyn phosphorylation and aggregation, neurite process disruption, and neuronal injury and cell death were all faithfully reproduced in the A53T-hiN culture system as found in human PD brains.[5–7] Additionally, using a second MS platform, our finding of similar aberrant S-nitrosylation reactions in TCA cycle enzymes in fresh-frozen postmortem human brain specimens from LBD patients as observed in A53T-hiN cultures supports the pathophysiological significance of our results. Thus, the hiPSC model system was useful for studying these features of synucleinopathy. It should be noted that our MS approaches to assessing protein S-nitrosylation are more sensitive and selective than prior biotin-switch assays, which have various caveats,[57–61] although our confirmatory biotin-switch blots largely confirmed our MS findings in the A53T-hiN. Another critical consideration in the analysis of metabolic experiments is concern over which compartments are being analyzed. In our case, we were able to discern the location of enzymes as mitochondrial vs. cytoplasmic via their exact amino-acid sequences obtained from the MS data for the protein S-nitrosylation experiments since the mitochondrial and cytoplasmic versions of these enzymes are in general not identical. Moreover, for the metabolic flux experiments, by focusing on the M+2 analysis after heavy isotope labeling of lactate, we limited our conclusions primarily to data obtained after one turn through the TCA cycle in order to focus on events primarily driven by entry into the TCA cycle via lactate and to avoid ancillary pathways of entry.

STAR★METHODS

RESOURCE AVAILABILITY

Lead contact—Further information and requests for resources and reagents should be directed to the lead contact, Stuart Lipton (slipton@scripps.edu).

Materials availability—Reagents generated in this study will be available upon request with a completed Materials Transfer Agreement.

Data and code availability

- The mass spectrometry proteomics data reported in this paper have been deposited at the ProteomeXchange Consortium (http://proteomecentral.proteomexchange.org) and are publicly available as of the date of publication. Accession numbers are listed in the key resources table.
- This paper does not report original code.

- Any additional information required to reanalyze the data reported in this paper is available from the lead contact upon request.

Experimental Model and Study Participant Details

hiPSC cultures—Pluripotent cells (hiPSCs) were cultured and maintained in our laboratory using a protocol described previously.[5,63] Briefly, hiPSCs were plated on γ-irradiated human foreskin fibroblasts and cultured using medium containing 20% KSR and 8 ng/ml bFGF, changed daily. The colonies were manually passaged weekly. Effects of the A53T mutation and PQ/MB were assessed in A9-type dopaminergic neurons differentiated from hiPSCs from two different genetic backgrounds; the two sets of isogenic cells (A53T mutant in the *SNCA* gene and gene-corrected WT/Control) were obtained from the laboratory of Rudolf Jaenisch at the Whitehead Institute of MIT[5,34] and from FujiFilm (iCell DopaNeurons PD SNCA A53T, C1113 and iCell DopaNeurons, C1028; FujiFilm Cellular Dynamics, Inc.).

hiN neuronal differentiation—We differentiated A53T and gene-corrected, isogenic WT/Control hiPSCs into A9-type dopaminergic neurons (hiN).[5,64] Briefly, just before differentiation,colonies were dissociated into a single cell suspensionusing accutase. To purify hiPSCs and remove fibroblast feeders, medium containing dissociated fibroblasts and hiPSCs was placed in gelatin-coated dishes. After adherence, supernatant containing purified hiPSCs was collected and re-plated at 4×10^4 cells/cm^2 on Matrigel (BD)-coated tissue culture dishes for differentiation. The floor-plate induction protocol was performed using medium containing knockout serum replacement (KSR), LDN193189 (100 nM), SB431542 (10 μM), sonic hedgehog (Shh) C25II (100 ng/ml), purmorphamine (2 μM), and CHIR99021 (3 μM). On day 5 of differentiation,KSR medium was slowly shifted to N2 medium (25%, 50%, 75%) every 2 days. At day 11, Neurobasal/B27/glutaMAX supplemented with CHIR medium was substituted. At day 13, CHIR was replaced with brain derived neurotrophic factor (BDNF; 20 ng ml^{-1}), ascorbic acid (0.2 mM), glial derived neurotrophic factor (GDNF; 20 ng ml^{-1}), transforming growth factor beta 3 (TGFβ3; 1 ng ml^{-1}), dibutyryl cAMP (db-cAMP; 0.5 mM), and DAPT (10 μM) for 9 days. At day 20, accutase was used to dissociate cells, which were re-plated at high cell density, 4×10^5 cells/cm^2 in terminal differentiation medium (NB/B27 + BDNF, ascorbic acid, GDNF, db cAMP, TGFβ3 and DAPT) or Dopaminergic Neuron (DAN) Medium on dishes pre-coated with poly-ornithine(15 μg/ml)/laminin (1 μg ml^{-1})/fibronectin (2 μg ml^{-1}). The resulting hiN were present in the absence of astrocyte feeders.

For hiN on a second genetic background, we used FujiFilm cells following the manufacturer's instructions with minor modifications. In brief, hiNs were seeded at 1.0 × 10^6 cells per well on 6-well plates and maintained in iCell Base Medium (FujiFilm Cellular Dynamics, M1010) containing 2% iCell Neural Supplement B (FujiFilm Cellular Dynamics, M1029) and 1% iCell Nervous System Supplement (FujiFilm Cellular Dynamics, M1031). Medium (50%) was replaced every 2–3 days. After 6 days, medium was changed to iCell Base Medium containing 2% B-27 Supplement minus antioxidants (ThermoFisher Scientific, 10889038) and incubated for 6 hr prior to exposure to vehicle or PQ/MB.

hiN were exposed to vehicle or to 2.8 μM PQ (Millipore Sigma, 36541)/1 μM MB (Millipore Sigma, 45554) for 16 h, as previously described[5].

Human LBD and control brains—Autopsy-confirmed human brains with LBD (n = 3 each females and males) and controls (n = 3 females/2 males) were matched for age, sex, education, and ethnicity (Table S2). Tissues were obtained from prefrontal cortex (Brodmann area 10). All brainswere obtained from the University of California (UCSD) Medical Center and the San Diego VA Medical Center Brain Bank and were flash frozen at postmortem examination. The study was approved by the local Ethics Committee of both medical centers. Neurological diagnoses were performed independently by two experienced clinicians using consensus criteria for LBD and were confirmed neuropathologically by the presence of Lewy bodies and Lewy neurites. All tissues were stored at −80 °C until use.

METHOD DETAILS

Metabolic flux and related experiments—PD/LBD and isogenic WT hiPSCs were prepared and differentiated into hiN as described above. Culture medium (2/3 volume) was exchanged biweekly with DAN medium, continuing for ~5 weeks. The final medium change contained 1 mM L-NAME (Millipore Sigma) for some wells for 24-h pretreatment. All wells were then switched for 6 h to Deprivation Medium (± L-NAME) containing B27/N2 supplements, but without glucose/pyruvate/lactate. To ascertain how lactate is handled by the TCA cycle in PD/LBD vs. WT hiN, 1 ml of 3X (30 mM) concentrations of either ^{12}C or ^{13}C-lactate (Cambridge Isotope Laboratories) in Deprivation Medium was added to the appropriate wells. After 6 h labeling, conditioned medium was harvested and snap frozen. Cells were washed once with PBS, solution aspirated, and cells snap frozen on the plates. Plates and media were then harvested for analysis of labeled metabolites to assess metabolic flux.

Metabolic flux analysis was performed by assessing ^{13}C-labeling of TCA intermediates in the Advanced Technology Core Facility at the Baylor College of Medicine using published protocols,[65–68] building on prior studies.[35,41–44] In brief homogenized samples were extracted in chloroform/methanol/water, and analysis was performed on a 6490 QQQ triple quadrupole mass spectrometer (Agilent Technologies) coupled to a 1290 Series HPLC system via selected reaction monitoring (SRM). Metabolites were targeted in both positive and negative ion modes with an electrospray source ionization (ESI) voltage of +4,000 V in the positive ion mode and – 3,500 V in the negative ion mode. For each detected metabolite, ~9–12 data points were collected. For the calculation of labeled metabolites, we used the equation (Mi*i)/n = Mi, the ratio of ^{13}C-labeled metabolite to the total pool, where i = M+x (i.e., M+2, M+3, etc., values) and n = number of carbons in the respective metabolite (e.g., for citrate = 6). M+x values can be summed to yield the molar percent enrichment (MPE), with molar enrichment (ME) equal to MPE times the total pool mean.

Kinetic model of ^{13}C-labeled TCA metabolites—Using tenets developed by Gupta et al.,[69] we constructed a semi-quantitative kinetic model for analysis of changes in metabolic flux through consecutive reactions of the TCA cycle in response to changes in the S-nitrosylation status of the corresponding enzymes. For multistep segments of the pathway

containing unmeasured metabolites, the consecutive reactions were reduced to a single step, containing only measured substrate and product, i.e., the segment between citrate and α-ketoglutarate was analyzed as if it were a single-step reaction catalyzed by a single enzymatic entity (that combines the activities of aconitase and isocitrate dehydrogenase since isocitrate was not measured in the mass spectrometric analysis). Similarly, a two-step conversion of α-ketoglutarate to succinate was considered as if a single step. The reaction rates (fluxes) were considered to follow mass-action law kinetics, consistent with the assumption that the substrate concentrations were much smaller in comparison to the corresponding Michaelis constant K_m for enzymatic reactions for the first turn through the TCA cycle. Accordingly, the flux through each step of the TCA cycle was assumed to be a product of substrate concentration and a corresponding kinetic constant and represent a pseudo first-order reaction process. These assumptions closely follow those utilized in the study by Gupta et al.[69]

The citrate synthase reaction represents an entry point into the TCA cycle for two-carbon moieties in the form of acetyl-CoA (Ac-CoA), and is, as such, a two-substrate reaction. We presumed a constant level of Ac-CoA as determined by a steady supply of carbons from a virtually unlimited pool of exogenously added lactate (10 mM in the bulk medium). Thus, the flux of the two-substrate reaction can be reduced to pseudo-first order form with observable kinetic constant k_1 equal to the product of two constants, $k_1 = k_1' \times [\text{Ac-CoA}]$, where k_1' is the actual kinetic constant for the two-substrate reaction.

Therefore, our model can be described by six elementary fluxes $J_i = k_i \times [A_i]$, corresponding to the six measured metabolites (citrate, α-ketoglutarate, succinate, fumarate, malate, and oxaloacetate). Here, [Ai] is the concentration of analyte number “i”, and ki is the kinetic constant for reaction of A_i, with i = 1, 2, …6. For each A_i, the rate of change is $d[A_i]/dt = J_{i-1} - J_i$. For example, malate is the fifth metabolite in the sequence, so the change in malate level $d[\text{malate}]/dt = J_4 - J_5 = k_4 \times [\text{fumarate}] - k_5 \times [\text{malate}]$; in other words, change in malate level equals the difference between malate production from fumarate and malate consumption in malate dehydrogenase reaction.

The initial pools of metabolites were set by a prolonged 6-hour starvation period when no source of two-carbon moieties (i.e., sucrose, pyruvate, nor lactate) were provided to the cells. The assumption was made under these conditions that all TCA cycle metabolites were converted to oxaloacetate and cannot be further converted due to lack of the second substrate of the citrate synthase reaction (Ac-CoA). Therefore, the initial condition for simulation was that the level of oxaloacetate equaled the total pool of TCA cycle metabolites, and all other metabolite levels were set to zero; all metabolites were unlabeled prior to the addition of ^{13}C-labeled lactate. Throughout the period of addition, all the entering two-carbon moieties were considered fully labeled, a reasonable assumption given such a high concentration (10 mM) of labeled lactate was provided.

Simulation of non-steady state kinetics was performed computationally. The model was applied recursively, starting from the initial conditions and changing the levels of each metabolite at each recursive step by an increment $\Delta[Ai]i \approx d[Ai]/dt$ to generate approximate theoretical kinetic curves for isotopologues of each metabolite. This approximation is valid

as long as the time increment corresponding to a recursion step is sufficiently small compared to the characteristic time of the total processes. As we were interested only in relative changes upon the biological perturbation triggered by the PD/LBD mutation A53T in the presence and absence of protein S-nitrosylation (the absence induced by the presence of L-NAME), we were free to select an arbitrary time scale that satisfies this assumption. Moreover, the control simulation implied perfectly balanced fluxes throughout all steps. For evaluation of responses to perturbation, the parameters of the model were manually fitted to produce changes in the ratios of consecutive metabolites ($[A_{i-1}]/[A_i]$) within 3% error of experimentally observed values upon challenge related to nitrosative stress.

Assessment of S-nitrosylation sites in cultured hiN—For assessment of the S-nitrosoproteome in cultured hiN, we used the established method of organomercury/chemoselective enrichment of S-nitrosothiols, which has been shown to be feasible and effective in such simplified culture models, as we recently described.[11] Experimental details for preparation and activation of columns, and reaction of homogenate with organomercury resin for S-nitrosocysteine enrichment have been presented previously.[45,46] For each group, five samples were analyzed with technical duplicates. For column washes, we used 50 bed volumes of 50 mM tris-HCl (pH 7.4), containing 300 mM NaCl and 0.5% SDS. Following this, 50 bed volumes of the same buffer containing 0.05% SDS were used. Next, columns were washed with 50 bed volumes of 50 mM tris-HCl containing 300 mM NaCl (pH 7.4), 1% Triton X-100, and 1 M urea. Columns were then washed with 50 bed volumes of the same buffer containing 0.1% Triton X-100 and 0.1 M urea, and finally 200 bed volumes of water. This was followed by on-column digestion into peptides; for this, columns were initially washed with 10 bed volumes of 0.1 M ammonium bicarbonate.

Bound proteins were then digested with Trypsin Gold (1 μg/mL) (Promega) that was added in a one bed volume of 0.1 M ammonium bicarbonate in the dark for 16 h at room temperature. Next, washing the resin with 40 bed volumes of 1 M ammonium bicarbonate (pH 7.4) containing 300 mM NaCl, and then 40 volumes of the same buffer without salt, 40 volumes of 0.1 M ammonium bicarbonate, and 200 volumes of deionized water. Bound peptides were eluted by treatment with one bed volume of performic acid in water.[45,70] To increase peptide recovery, the column was further washed with one volume of deionized water. The eluted peptides thus obtained were stored at −80 °C overnight, and then lyophilized and resuspended in a 300 μL volume of 0.1% formic acid. The peptides in the resuspended solution were put in low-retention tubes (Axygen) and the volume reduced to 30 μL by speed vacuum. Peptides were then desalted using Stage Tips (ThermoFisher) and transferred to a high-performance liquid chromatography (LC) vial for subsequent LC-tandem mass spectrometry (MS/MS) analysis of SNO-peptides using a Orbitrap Elite Hybrid Ion Trap-Orbitrap Mass Spectrometer (ThermoFisher). As previously described,[70] we determined the S-nitrosoproteome by identifying S-nitrosylated peptides and proteins for each sample group.

Five different biological samples per group were analyzed in duplicate. The last step for the organomercury-based site-specific identification of S-nitrosylated cysteine residues consists of using mild performic acid to release the bound peptides selectively and quantitatively. Importantly, the performic acid oxidizes the cysteine thiols to sulfonic acid,

thereby generating a unique MS signature that permits site-specific identification of the modified cysteine residues as >96% of cysteine-containing peptides were detected with the sulfonic acid modification in the 20 samples analyzed. For the final reporting table all peptides detected in the duplicate samples for each condition were grouped.[60] Note that the organomercury/chemoselective method identifies the sites of S-nitrosylation by detecting peptides with modified cysteine residues. Since, like other protein posttranslational modifications, S-nitrosylation is sub-stoichiometric, some peptides will not be captured and detected. In this regard, the presence of a particular peptide in one biological condition (e.g., control cells) and its absence from another can be attributed to the following possible reasons: The cysteine residue is not S-nitrosylated, or its S-nitrosylation level is below the detection limit of the method.

Biotin-switch assay in hiN for SNO-TCA enzymes—Biotin-switch assays were performed as described previously.[51,52] In brief, hiN lysates were prepared in HEN buffer [100 mM HEPES-NaOH (pH 7.4), 1 mM EDTA, 0.1 mM neocuproine] containing 150 mM NaCl, 1% NP-40, 0.5% deoxycholate, and 0.1% SDS. Free thiol groups were blocked by 10 mM S-methyl methanethiosulfonate (MMTS, Millipore Sigma, 208795) in HEN buffer for 20 min at 42 °C. After removing excess MMTS by acetone precipitation, S-nitrosothiols were specifically reduced to free thiols using freshly prepared, 10 mM sodium ascorbate (Millipore Sigma, 11140), and the newly formed free thiols were labeled with 1 mM Biotin-HPDP (WS) (Dojindo Molecular Technologies, SB17) for 1 h at RT. Biotinylated proteins were enriched by High Capacity NeutrAvidin Agarose (ThermoFisher Scientific, 29204). The purified biotinylated proteins were then eluted from beads for immunoblot analysis.

For immunoblotting, samples were subjected to Bolt 4–12% Bis-Tris mini protein gels (ThermoFisher Scientific, NW04122BOX) and transferred to Immobilon-FL PVDF membranes (Millipore Sigma, IPFL00010). The membranes were blocked with Intercept TBS blocking buffer (Li-Cor, 927–60001) and incubated overnight at 4 °C with primary antibodies against lipoamide dehydrogenase (DLD, Abcam, ab133551) and Aconitase 2 (Aco2 or AC, Cell Signaling Technologies, 6922S). After 3 washes with 1X TBS-T (Cell Signaling Technology, 9997S), the membranes were incubated with IR-dye-conjugated secondary antibody (IR-dye 800CW-conjugated goat anti-rabbit [1:15,000; Li-Cor, 926–32211]) for 1 h at RT. Membranes were scanned with an Odyssey CLx infrared imaging system (Li-Cor). Image Studio software (Li-Cor) was used for densitometric analysis of immunoblots.

Preparation of human brains for mass spectrometry—Brain tissues were homogenized on ice using a Teflon pestle and a Jumbo Stirrer (ThermoFisher) in freshly prepared lysis buffer (100 mM HEPES-NaOH, pH 7.7, 1 mM EDTA, 0.1 mM neocuproine, 1% Triton X-100, 20 mM IAM, 1% protease inhibitor cocktail, and 0.1% SDS). Homogenates were then centrifuged at 16,000 g for 15 min at 4 °C, and supernatants collected. Protein concentration was determined by the Bradford assay. One volume of 50 mM HEPES buffer (pH 7.7) was added to the supernatants, which were then centrifuged at 5,000 g for 25 min at 4 °C using 10 K MWCO spin filters.

For assessment of the S-nitrosoproteome in brain tissue, we used the established *SNO*TRAP technique with triaryl phosphine-based labeling of S-nitrosothiols, which we have shown to be feasible and effective on complicated mixtures of cell types and proteins.[61,71] *SNO*TRAP-labeling stock solutions prepared in acetonitrile (ACN) were added to samples at a final concentration of 1.5 mM to selectively convert SNO to stable disulfide-iminophosphorane. For negative controls, we doped the same volume of 40% ACN in 50 mM HEPES (pH 7.7). The samples were incubated at RT for 2 h. After reaction, excessive reagents were removed with three washes of 50 mM HEPES, pH 7.7 buffer with 10 K MWCO filters, followed by trypsin digestion overnight at 37 °C.

After enzymatic digestion into peptides, 200 μL Streptavidin agarose beads were added to each sample and incubated for 2 h at RT with gentle shaking. To minimize non-specific binding, the beads were washed twice with 5-fold volumes of the following buffers in succession: Buffer I (100 mM NH_4HCO_3 (ABC), 150 mM NaCl, 1 mM EDTA, pH 7.4, containing 0.05% SDS, 0.1% Triton X-100); buffer II (100 mM ABC, 150 mM NaCl, 1 mM EDTA, pH 7.4 containing 0.1% SDS); buffer III (100 mM ABC + 0.05% SDS + 150 mM NaCl), buffer IV (100 mM ABC), and buffer V (50 mM HEPES, pH 7.7). Peptides bound to beads were then eluted with 10 mM TCEP (in 50 mM HEPES, pH 7.7) and alkylated with 100 mM NEM for 2 h at RT. After alkylation, samples were desalted with Pierce C18 spin columns and stored at –80 °C prior to analysis. Sample preparation and storage were conducted in the dark.

NanoLC-MS analysis of *SNO*TRAP-labeled brain samples—The desalted peptides, dissolved in 0.1% FA, were analyzed using a Q Exactive mass spectrometer coupled to Easy-nLC 1000 (ThermoFisher Scientific, Waltham, MA) interfaced via a nanoSpray Flex ion source. Five technical runs were conducted for each biological replicate, i.e., from tissue of a single individual. Formic acid in water (0.1%) and in ACN (0.1%) were used as mobile phases A and B, respectively. Aliquots (3 μL) of the samples were injected onto a C18 pre-column (75 μm ID × 20 mm, 3 μm, ThermoFisher Scientific) and separated by a C18 column (75 μm ID × 250 mm, 2 μm, ThermoFisher Scientific) with a stepwise gradient (1% B for 10 min, 1–60% B for 110 min, and then 60–100% B for 10 min) followed by a 10 min post-run at 1% B at a flow rate of 300 nL/min. Mass spectra were acquired in data-dependent mode using the following settings: spray voltage, 2.2 kV; capillary temperature, 250 °C; S-lens RF level, 60%; no sheath and auxiliary gas flow; resolution 70,000; scan range 350–1800 Th. The 10 most abundant ions with multiple charge-states were selected for fragmentation with an isolation window of 2 Th, and a normalized collision energy of 28% at a resolution of 35,000. The maximum ion injection times for the full MS scan and the MS/MS scan were both 100 ms. The ion target values for the full scan and the MS/MS scans were set to 3×10^6 and 1×10^5, respectively. Xcalibur software was used for data acquisition.

MS data processing of human brain S-nitrosoproteome—Agilent Spectrum Mill MS proteomics Workbench B.06 was used for peak list generation, database searching, label-free semiquantitative assessment, and false discovery rate (FDR) estimation. Parameters for data extractions were as follows: Precursor MH^+ 300 – 8000 Da, scan

time range 0–200 min, sequence tag length > 1, merge scans with same precursor *m/z* ±30s and ±0.05 *m/z*, default for precursor charge, true for find ^{12}C precursor, MS noise threshold 100 counts. MS/MS spectra were searched against the human SwissProt protein database (downloaded on 06/18/2019) with ±10 ppm precursor ion tolerance and ± 20 ppm fragment ion tolerance. The search included variable modifications of methionine oxidation, protein N-terminal acetylation, deamidation of asparagine, and fixed modification of N-ethylmaleimide on Cys. For both peptide identification and protein polishing, the FDR was set to 1%. Peptide identifications were accepted only if the following confidence thresholds were met: Minimal peptide length was set to five amino acids, and a maximum of two missed cleavages was allowed. The MS/MS spectra were inspected manually to validate the peptide/protein identifications. In addition, for proteins detected in one group but not another, the raw LC/MS data files for the latter were searched manually for the presence of protein-related peptides detected in the former. The MS raw data have been deposited in the ProteomeXchange Consortium (http://proteomecentral.proteomexchange.org) via the PRIDE partner repository with the dataset identifiers PXD036703 and PXD036797.

Statistical analyses of S-nitrosylated proteins—For S-nitrosoproteins identified in brain with the *SNO*TRAP technique, the precursor intensities of SNO-proteins, estimated in Spectrum Mill by combining precursor intensities of the constituent peptides in MS1 spectra, were used to calculate fold-change quantification of the common SNO-proteins detected in disease and control groups, with fold-change defined as total-ion intensity LBD sample divided by total-ion intensity of respective control. Statistical evaluation of nanoLC-MS label-free differential data was performed after the application of data imputation to reduce the number of missing values. Missing values were replaced by this value according to the local Minimum method.[72] A fold change of >2 was considered increased expression, while fold change of <0.5, decreased expression; these cut-offs corresponded to a p-value < 0.05, as we have described previously.[61] For comparison of approximate quantifications of SNO-proteins obtained with Spectrum Mill, a non-parametric Kruskal-Wallis statistical test was used.

For S-nitrosoproteins identified by organomercury/chemoselective enrichment, after column digestion to generate peptides and elution of peptides, the trioxidation of SNO-cysteine residues was used to identify the site of modification). Raw MS data were analyzed with MaxQuant open-source software using cysteine trioxidation and methionine dioxidation as differential modifications. We report the S-nitrosylation sites on the peptides/proteins based on the MaxQuant output.

Bioinformatics of S-nitrosoproteome data—To analyze functional enrichment of gene ontology (GO) processes and pathways for the human LBD vs. control brains characterized by *SNO*TRAP, we uploaded the SNO-protein IDs into MetaCore™ software (version 19.4 build 69900). Reactome pathway analysis was performed using STRING (version 11.0) (http://string-db.org).[73] High reliability interactions (score > 0.7) were analyzed. To visualize protein-protein interactions, we used Cytoscape plug-in software (version 3.7.2). FDR values <0.1 were accepted for the analyses using the aforementioned software platforms. The gene names for the unique proteins identified for each of the

six conditions were submitted to Gene Ontology http://geneontology.org and analyzed for functional processes or cellular component (localization) enrichment.

Following S-nitrosoproteome identification in hiN by organomercury/chemoselective enrichment, functional analysis was performed to characterize the biological pathways affected using gene ontology (GO) knowledgebase (2020–12-08 release) enrichment, pathway analysis using the Kyoto Encyclopedia of Genes and Genomes (KEGG release 96.0, October 1, 2020), and STRING protein-protein interaction network functional enrichment as we have described.[11]

QUANTIFICATION AND STATISTICAL ANALYSIS

Data were analyzed with the tests indicated in the appropriate paragraph for statistical analysis and bioinformatics (see above). For analysis of S-nitrosylated proteins, the number of samples analyzed are indicated in the methods and main text. For metabolic flux data, n numbers for biological replicates are included in the figure legends; comparisons were made by ANOVA followed by a PLSD post hoc test.[62] For comparison of S-nitrosylated protein/total protein ratios, an ANOVA with post hoc Tukey test was performed, as previously.[52] For both the analysis of S-nitrosylated proteins and metabolic flux data, a p-value ≤ 0.05 was considered significant.

Supplementary Material

Refer to Web version on PubMed Central for supplementary material.

ACKNOWLEDGMENTS

We are indebted to Christian Metallo (Salk Institute), Itzhak Nissim (University of Pennsylvania), and John Essigmann (MIT) for helpful discussions and advice on the analysis of the metabolic flux results. We gratefully acknowledge access to the Baylor College of Medicine Advanced Technology Core directed by Nagireddy Putluri and thank Vasanta Putluri, who ran our metabolic flux experiments. We thank Eliezer Masliah (UC San Diego/NIA) and Robert Rissman (UC San Diego) for providing human brain tissues as part of the NIH supported National AD/ADRD Brain Bank. We thank Hossein Fazelinia, Ding Hua, and Lynn Spruce at the Proteomics Core Facility of the Children's Hospital of Philadelphia, for their support and discussions regarding the MS-based proteomic analyses. This study was supported in part by NIH grants R01AG056259 (to S.R.T.), R01 AG061845, R61 NS122098, and RF1 NS123298 (to T.N.), and R35 AG071734, RF1 AG057409, R01 AG056259, R56 AG065372, R01 DA048882 and DP1 DA041722 (to S.A.L.) and R01 AG056259 (to S.A.L. and S.R.T.). H.I. is the Gisela and Dennis Alter Research Professor at the Children's Hospital of Philadelphia Research Institute.

INCLUSION AND DIVERSITY

We support inclusive, diverse, and equitable conduct of research.

REFERENCES

1. Exner N, Lutz AK, Haass C, and Winklhofer KF (2012). Mitochondrial dysfunction in Parkinson's disease: molecular mechanisms and pathophysiological consequences. EMBO J. 31, 3038–3062. 10.1038/emboj.2012.170. [PubMed: 22735187]
2. Vazquez-Velez GE, and Zoghbi HY (2021). Parkinson's disease genetics and pathophysiology. Annu. Rev. Neurosci. 44, 87–108. 10.1146/annurev-neuro-100720-034518. [PubMed: 34236893]
3. Cooper O, Seo H, Andrabi S, Guardia-Laguarta C, Graziotto J, Sundberg M, McLean JR, Carrillo-Reid L, Xie Z, Osborn T, et al. (2012). Pharmacological rescue of mitochondrial deficits in iPSC-

derived neural cells from patients with familial Parkinson's disease. Sci. Transl. Med. 4, 141ra190. 10.1126/scitranslmed.3003985.

4. Chung CY, Khurana V, Auluck PK, Tardiff DF, Mazzulli JR, Soldner F, Baru V, Lou Y, Freyzon Y, Cho S, et al. (2013). Identification and rescue of α-synuclein toxicity in Parkinson patient-derived neurons. Science 342, 983–987. 10.1126/science.1245296. [PubMed: 24158904]
5. Ryan SD, Dolatabadi N, Chan SF, Zhang X, Akhtar MW, Parker J, Soldner F, Sunico CR, Nagar S, Talantova M, et al. (2013). Isogenic human iPSC Parkinson's model shows nitrosative stress-induced dysfunction in MEF2-PGC1α transcription. Cell 155, 1351–1364. 10.1016/j.cell.2013.11.009. [PubMed: 24290359]
6. Ryan T, Bamm VV, Stykel MG, Coackley CL, Humphries KM, Jamieson-Williams R, Ambasudhan R, Mosser DD, Lipton SA, Harauz G, and Ryan SD (2018). Cardiolipin exposure on the outer mitochondrial membrane modulates α-synuclein. Nat. Commun. 9, 817. 10.1038/s41467-018-03241-9. [PubMed: 29483518]
7. Czaniecki C, Ryan T, Stykel MG, Drolet J, Heide J, Hallam R, Wood S, Coackley C, Sherriff K, Bailey CDC, and Ryan SD (2019). Axonal pathology in hPSC-based models of Parkinson's disease results from loss of Nrf2 transcriptional activity at the Map1b gene locus. Proc. Natl. Acad. Sci. USA 116, 14280–14289. 10.1073/pnas.1900576116. [PubMed: 31235589]
8. Trudler D, Sanz-Blasco S, Eisele YS, Ghatak S, Bodhinathan K, Akhtar MW, Lynch WP, Pina-Crespo JC, Talantova M, Kelly JW, and Lipton SA (2021). A-Synuclein oligomers induce glutamate release from astrocytes and excessive extrasynaptic NMDAR Activity in neurons, thus contributing to synapse loss. J. Neurosci. 41, 2264–2273. 10.1523/JNEUROSCI.1871-20.2020. [PubMed: 33483428]
9. Caminiti SP, Sala A, Iaccarino L, Beretta L, Pilotto A, Gianolli L, Iannaccone S, Magnani G, Padovani A, Ferini-Strambi L, and Perani D (2019). Brain glucose metabolism in Lewy body dementia: implications for diagnostic criteria. Alzheimers Res Ther 11, 20. 10.1186/s13195-019-0473-4. [PubMed: 30797240]
10. Gibson GE, Starkov A, Blass JP, Ratan RR, and Beal MF (2010). Cause and consequence: mitochondrial dysfunction initiates and propagates neuronal dysfunction, neuronal death and behavioral abnormalities in age-associated neurodegenerative diseases. Biochim. Biophys. Acta 1802, 122–134. 10.1016/j.bbadis.2009.08.010. [PubMed: 19715758]
11. Doulias PT, Nakamura T, Scott H, McKercher SR, Sultan A, Deal A, Albertolle M, Ischiropoulos H, and Lipton SA (2021). TCA cycle metabolic compromise due to an aberrant S-nitrosoproteome in HIV-associated neurocognitive disorder with methamphetamine use. J. Neurovirol. 27, 367–378. 10.1007/s13365-021-00970-4. [PubMed: 33876414]
12. Kam TI, Mao X, Park H, Chou SC, Karuppagounder SS, Umanah GE, Yun SP, Brahmachari S, Panicker N, Chen R, et al. (2018). Poly(ADP-ribose) drives pathologic α-synuclein neurodegeneration in Parkinson's disease. Science 362, eaat8407. 10.1126/science.aat8407. [PubMed: 30385548]
13. Bolanos JP, Peuchen S, Heales SJ, Land JM, and Clark JB (1994). Nitric oxide-mediated inhibition of the mitochondrial respiratory chain in cultured astrocytes. J. Neurochem. 63, 910–916. 10.1046/j.1471-4159.1994.63030910.x. [PubMed: 7519665]
14. Brown GC, and Cooper CE (1994). Nanomolar concentrations of nitric oxide reversibly inhibit synaptosomal respiration by competing with oxygen at cytochrome oxidase. FEBS Lett. 356, 295–298. 10.1016/0014-5793(94)01290-3. [PubMed: 7805858]
15. Schweizer M, and Richter C (1994). Nitric oxide potently and reversibly deenergizes mitochondria at low oxygen tension. Biochem. Biophys. Res. Commun. 204, 169–175. 10.1006/bbrc.1994.2441. [PubMed: 7945356]
16. Clementi E, Brown GC, Feelisch M, and Moncada S (1998). Persistent inhibition of cell respiration by nitric oxide: crucial role of S-nitrosylation of mitochondrial complex I and protective action of glutathione. Proc. Natl. Acad. Sci. USA 95, 7631–7636. 10.1073/pnas.95.13.7631. [PubMed: 9636201]
17. Beltran B, Orsi A, Clementi E, and Moncada S (2000). Oxidative stress and S-nitrosylation of proteins in cells. Br. J. Pharmacol. 129, 953–960. 10.1038/sj.bjp.0703147. [PubMed: 10696095]

18. Almeida A, Almeida J, Bolanos JP, and Moncada S (2001). Different responses of astrocytes and neurons to nitric oxide: the role of glycolytically generated ATP in astrocyte protection. Proc. Natl. Acad. Sci. USA 98, 15294–15299. 10.1073/pnas.261560998. [PubMed: 11742096]
19. Stewart VC, and Heales SJ (2003). Nitric oxide-induced mitochondrial dysfunction: implications for neurodegeneration. Free Radic. Biol. Med. 34, 287–303. 10.1016/s0891-5849(02)01327-8. [PubMed: 12543245]
20. Antunes F, Boveris A, and Cadenas E (2004). On the mechanism and biology of cytochrome oxidase inhibition by nitric oxide. Proc. Natl. Acad. Sci. USA 101, 16774–16779. 10.1073/pnas.0405368101. [PubMed: 15546991]
21. Cooper CE, and Giulivi C (2007). Nitric oxide regulation of mitochondrial oxygen consumption II: Molecular mechanism and tissue physiology. Am. J. Physiol. Cell Physiol. 292, C1993–2003. 10.1152/ajpcell.00310.2006. [PubMed: 17329402]
22. Ledo A, Barbosa R, Cadenas E, and Laranjinha J (2010). Dynamic and interacting profiles of *NO and O2 in rat hippocampal slices. Free Radic. Biol. Med. 48, 1044–1050. 10.1016/j.freeradbiomed.2010.01.024. [PubMed: 20100565]
23. Martinez-Ruiz A, Cadenas S, and Lamas S (2011). Nitric oxide signaling: classical, less classical, and nonclassical mechanisms. Free Radic. Biol. Med. 51, 17–29. 10.1016/j.freeradbiomed.2011.04.010. [PubMed: 21549190]
24. San Martin A, Arce-Molina R, Galaz A, Perez-Guerra G, and Barros LF (2017). Nanomolar nitric oxide concentrations quickly and reversibly modulate astrocytic energy metabolism. J. Biol. Chem. 292, 9432–9438. 10.1074/jbc.M117.777243. [PubMed: 28341740]
25. Laranjinha J, Nunes C, Ledo A, Lourenco C, Rocha B, and Barbosa RM (2021). The peculiar facets of nitric oxide as a cellular messenger: From disease-associated signaling to the regulation of brain bioenergetics and neurovascular coupling. Neurochem. Res. 46, 64–76. 10.1007/s11064-020-03015-0. [PubMed: 32193753]
26. Zheng X, Boyer L, Jin M, Mertens J, Kim Y, Ma L, Ma L, Hamm M, Gage FH, and Hunter T (2016). Metabolic reprogramming during neuronal differentiation from aerobic glycolysis to neuronal oxidative phosphorylation. Elife 5, e13374. 10.7554/eLife.13374. [PubMed: 27282387]
27. Pellerin L, and Magistretti PJ (1994). Glutamate uptake into astrocytes stimulates aerobic glycolysis: a mechanism coupling neuronal activity to glucose utilization. Proc. Natl. Acad. Sci. USA 91, 10625–10629. 10.1073/pnas.91.22.10625. [PubMed: 7938003]
28. Magistretti PJ, and Allaman I (2015). A cellular perspective on brain energy metabolism and functional imaging. Neuron 86, 883–901. 10.1016/j.neuron.2015.03.035. [PubMed: 25996133]
29. Magistretti PJ, and Allaman I (2018). Lactate in the brain: from metabolic end-product to signalling molecule. Nat. Rev. Neurosci. 19, 235–249. 10.1038/nrn.2018.19. [PubMed: 29515192]
30. Diaz-Garcia CM, Mongeon R, Lahmann C, Koveal D, Zucker H, and Yellen G (2017). Neuronal stimulation triggers neuronal glycolysis and not lactate uptake. Cell Metab. 26, 361–374 e364. 10.1016/j.cmet.2017.06.021. [PubMed: 28768175]
31. Li S, and Sheng ZH (2022). Energy matters: presynaptic metabolism and the maintenance of synaptic transmission. Nat. Rev. Neurosci. 23, 4–22. 10.1038/s41583-021-00535-8. [PubMed: 34782781]
32. Cheng XT, Huang N, and Sheng ZH (2022). Programming axonal mitochondrial maintenance and bioenergetics in neurodegeneration and regeneration. Neuron 110, 1899–1923. 10.1016/j.neuron.2022.03.015. [PubMed: 35429433]
33. Dembitskaya Y, Piette C, Perez S, Berry H, Magistretti PJ, and Venance L (2022). Lactate supply overtakes glucose when neural computational and cognitive loads scale up. Proc. Natl. Acad. Sci. USA 119, e2212004119. 10.1073/pnas.2212004119. [PubMed: 36375086]
34. Soldner F, Laganiere J, Cheng AW, Hockemeyer D, Gao Q, Alagappan R, Khurana V, Golbe LI, Myers RH, Lindquist S, et al. (2011). Generation of isogenic pluripotent stem cells differing exclusively at two early onset Parkinson point mutations. Cell 146, 318–331. 10.1016/j.cell.2011.06.019. [PubMed: 21757228]
35. Ruiz M, Gelinas R, Vaillant F, Lauzier B, and Des Rosiers C (2015). Metabolic tracing using stable isotope-labeled substrates and mass spectrometry in the perfused mouse heart. Methods Enzymol. 561, 107–147. 10.1016/bs.mie.2015.06.026. [PubMed: 26358903]

36. Cordes T, and Metallo CM (2019). Quantifying intermediary metabolism and lipogenesis in cultured mammalian cells using stable isotope tracing and mass spectrometry. Methods Mol. Biol. 1978, 219–241. 10.1007/978-1-4939-9236-2_14.
37. Torrini C, Nguyen TTT, Shu C, Mela A, Humala N, Mahajan A, Seeley EH, Zhang G, Westhoff MA, Karpel-Massler G, et al. (2022). Lactate is an epigenetic metabolite that drives survival in model systems of glioblastoma. Mol. Cell 82, 3061–3076 e3066. 10.1016/j.molcel.2022.06.030. [PubMed: 35948010]
38. Fernandez-Garcia J, Altea-Manzano P, Pranzini E, and Fendt SM (2020). Stable isotopes for tracing mammalian-cell metabolism *in vivo*. Trends Biochem. Sci. 45, 185–201. 10.1016/j.tibs.2019.12.002. [PubMed: 31955965]
39. Nakamura T, and Lipton SA (2017). 'SNO'-storms compromise protein activity and mitochondrial metabolism in neurodegenerative disorders. Trends Endocrinol. Metab. 28, 879–892. 10.1016/j.tem.2017.10.004. [PubMed: 29097102]
40. Liu T, Zhang M, Mukosera GT, Borchardt D, Li Q, Tipple TE, Ishtiaq Ahmed AS, Power GG, and Blood AB (2019). L-NAME releases nitric oxide and potentiates subsequent nitroglycerin-mediated vasodilation. Redox Biol. 26, 101238. 10.1016/j.redox.2019.101238. [PubMed: 31200239]
41. Lewis CA, Parker SJ, Fiske BP, McCloskey D, Gui DY, Green CR, Vokes NI, Feist AM, Vander Heiden MG, and Metallo CM (2014). Tracing compartmentalized NADPH metabolism in the cytosol and mitochondria of mammalian cells. Mol. Cell 55, 253–263. 10.1016/j.molcel.2014.05.008. [PubMed: 24882210]
42. Buescher JM, Antoniewicz MR, Boros LG, Burgess SC, Brunengraber H, Clish CB, DeBerardinis RJ, Feron O, Frezza C, Ghesquiere B, et al. (2015). A roadmap for interpreting (13)C metabolite labeling patterns from cells. Curr. Opin. Biotechnol. 34, 189–201. 10.1016/j.copbio.2015.02.003. [PubMed: 25731751]
43. Jang C, Chen L, and Rabinowitz JD (2018). Metabolomics and isotope tracing. Cell 173, 822–837. 10.1016/j.cell.2018.03.055. [PubMed: 29727671]
44. Butterfield DA, and Halliwell B (2019). Oxidative stress, dysfunctional glucose metabolism and Alzheimer disease. Nat. Rev. Neurosci. 20, 148–160. 10.1038/s41583-019-0132-6. [PubMed: 30737462]
45. Doulias PT, Greene JL, Greco TM, Tenopoulou M, Seeholzer SH, Dunbrack RL, and Ischiropoulos H (2010). Structural profiling of endogenous S-nitrosocysteine residues reveals unique features that accommodate diverse mechanisms for protein S-nitrosylation. Proc. Natl. Acad. Sci. USA 107, 16958–16963. 10.1073/pnas.1008036107. [PubMed: 20837516]
46. Doulias PT, Tenopoulou M, Raju K, Spruce LA, Seeholzer SH, and Ischiropoulos H (2013). Site specific identification of endogenous S-nitrosocysteine proteomes. J. Proteomics 92, 195–203. 10.1016/j.jprot.2013.05.033. [PubMed: 23748021]
47. Bruegger JJ, Smith BC, Wynia-Smith SL, and Marletta MA (2018). Comparative and integrative metabolomics reveal that S-nitrosation inhibits physiologically relevant metabolic enzymes. J. Biol. Chem. 293, 6282–6296. 10.1074/jbc.M117.817700. [PubMed: 29483187]
48. Gonzalez-Rodriguez P, Zampese E, Stout KA, Guzman JN, Ilijic E, Yang B, Tkatch T, Stavarache MA, Wokosin DL, Gao L, et al. (2021). Disruption of mitochondrial complex I induces progressive parkinsonism. Nature 599, 650–656. 10.1038/s41586-021-04059-0. [PubMed: 34732887]
49. von Bartheld CS, Bahney J, and Herculano-Houzel S (2016). The search for true numbers of neurons and glial cells in the human brain: A review of 150 years of cell counting. J. Comp. Neurol. 524, 3865–3895. 10.1002/cne.24040. [PubMed: 27187682]
50. Uehara T, Nakamura T, Yao D, Shi ZQ, Gu Z, Ma Y, Masliah E, Nomura Y, and Lipton SA (2006). S-Nitrosylated protein-disulphide isomerase links protein misfolding to neurodegeneration. Nature 441, 513–517. 10.1038/nature04782. [PubMed: 16724068]
51. Cho DH, Nakamura T, Fang J, Cieplak P, Godzik A, Gu Z, and Lipton SA (2009). S-Nitrosylation of Drp1 mediates β-amyloid-related mitochondrial fission and neuronal injury. Science 324, 102–105. 10.1126/science.1171091. [PubMed: 19342591]

52. Nakamura T, Oh CK, Liao L, Zhang X, Lopez KM, Gibbs D, Deal AK, Scott HR, Spencer B, Masliah E, et al. (2021). Noncanonical transnitrosylation network contributes to synapse loss in Alzheimer's disease. Science 371, eaaw0843. 10.1126/science.aaw0843. [PubMed: 33273062]
53. Akhtar MW, Sanz-Blasco S, Dolatabadi N, Parker J, Chon K, Lee MS, Soussou W, McKercher SR, Ambasudhan R, Nakamura T, and Lipton SA (2016). Elevated glucose and oligomeric β-amyloid disrupt synapses via a common pathway of aberrant protein S-nitrosylation. Nat. Commun. 7, 10242. 10.1038/ncomms10242. [PubMed: 26743041]
54. Barsoum MJ, Yuan H, Gerencser AA, Liot G, Kushnareva Y, Graber S, Kovacs I, Lee WD, Waggoner J, Cui J, et al. (2006). Nitric oxide-induced mitochondrial fission is regulated by dynamin-related GTPases in neurons. EMBO J. 25, 3900–3911. 10.1038/sj.emboj.7601253. [PubMed: 16874299]
55. Nakamura T, and Lipton SA (2020). Nitric oxide-dependent protein post-translational modifications impair mitochondrial function and metabolism to contribute to neurodegenerative diseases. Antioxid. Redox Signal. 32, 817–833. 10.1089/ars.2019.7916. [PubMed: 31657228]
56. Bhaduri A, Andrews MG, Kriegstein AR, and Nowakowski TJ (2020). Are organoids ready for prime time? Cell Stem Cell 27, 361–365. 10.1016/j.stem.2020.08.013. [PubMed: 32888425]
57. Forrester MT, Foster MW, and Stamler JS (2007). Assessment and application of the biotin switch technique for examining protein S-nitrosylation under conditions of pharmacologically induced oxidative stress. J. Biol. Chem. 282, 13977–13983. 10.1074/jbc.M609684200. [PubMed: 17376775]
58. Forrester MT, Foster MW, Benhar M, and Stamler JS (2009). Detection of protein S-nitrosylation with the biotin-switch technique. Free Radic. Biol. Med. 46, 119–126. 10.1016/j.freeradbiomed.2008.09.034. [PubMed: 18977293]
59. Wang Y, Liu T, Wu C, and Li H (2008). A strategy for direct identification of protein S-nitrosylation sites by quadrupole time-of-flight mass spectrometry. J. Am. Soc. Mass Spectrom. 19, 1353–1360. 10.1016/j.jasms.2008.06.001. [PubMed: 18635375]
60. Raju K, Doulias PT, Evans P, Krizman EN, Jackson JG, Horyn O, Daikhin Y, Nissim I, Yudkoff M, Nissim I, et al. (2015). Regulation of brain glutamate metabolism by nitric oxide and S-nitrosylation. Sci. Signal. 8, ra68. 10.1126/scisignal.aaa4312. [PubMed: 26152695]
61. Seneviratne U, Nott A, Bhat VB, Ravindra KC, Wishnok JS, Tsai LH, and Tannenbaum SR (2016). S-nitrosation of proteins relevant to Alzheimer's disease during early stages of neurodegeneration. Proc. Natl. Acad. Sci. USA 113, 4152–4157. 10.1073/pnas.1521318113. [PubMed: 27035958]
62. Frane A (2019). Type I error control in psychology research: Improving understanding in general and addressing multiplicity in some specific contexts. (UCLA).
63. Lin T, Ambasudhan R, Yuan X, Li W, Hilcove S, Abujarour R, Lin X, Hahm HS, Hao E, Hayek A, and Ding S (2009). A chemical platform for improved induction of human iPSCs. Nat. Methods 6, 805–808. 10.1038/nmeth.1393. [PubMed: 19838168]
64. Kriks S, Shim JW, Piao J, Ganat YM, Wakeman DR, Xie Z, Carrillo-Reid L, Auyeung G, Antonacci C, Buch A, et al. (2011). Dopamine neurons derived from human ES cells efficiently engraft in animal models of Parkinson's disease. Nature 480, 547–551. 10.1038/nature10648. [PubMed: 22056989]
65. Vantaku V, Donepudi SR, Ambati CR, Jin F, Putluri V, Nguyen K, Rajapakshe K, Coarfa C, Battula VL, Lotan Y, and Putluri N (2017). Expression of ganglioside GD2, reprogram the lipid metabolism and EMT phenotype in bladder cancer. Oncotarget 8, 95620–95631. 10.18632/oncotarget.21038. [PubMed: 29221154]
66. Jin F, Thaiparambil J, Donepudi SR, Vantaku V, Piyarathna DWB, Maity S, Krishnapuram R, Putluri V, Gu F, Purwaha P, et al. (2017). Tobacco-specific carcinogens induce hypermethylation, DNA adducts, and DNA damage in bladder cancer. Cancer Prev. Res. (Phila) 10, 588–597. 10.1158/1940-6207.CAPR-17-0198. [PubMed: 28851690]
67. Piyarathna DWB, Rajendiran TM, Putluri V, Vantaku V, Soni T, von Rundstedt FC, Donepudi SR, Jin F, Maity S, Ambati CR, et al. (2018). Distinct lipidomic landscapes associated with clinical stages of urothelial cancer of the bladder. Eur. Urol. Focus 4, 907–915. 10.1016/j.euf.2017.04.005. [PubMed: 28753886]

68. Kornberg MD, Bhargava P, Kim PM, Putluri V, Snowman AM, Putluri N, Calabresi PA, and Snyder SH (2018). Dimethyl fumarate targets GAPDH and aerobic glycolysis to modulate immunity. Science 360, 449–453. 10.1126/science.aan4665. [PubMed: 29599194]

69. Gupta S, Maurya MR, Stephens DL, Dennis EA, and Subramaniam S (2009). An integrated model of eicosanoid metabolism and signaling based on lipidomics flux analysis. Biophys. J. 96, 4542–4551. 10.1016/j.bpj.2009.03.011. [PubMed: 19486676]

70. Doulias PT, Tenopoulou M, Greene JL, Raju K, and Ischiropoulos H (2013). Nitric oxide regulates mitochondrial fatty acid metabolism through reversible protein S-nitrosylation. Sci. Signal. 6, rs1. 10.1126/scisignal.2003252. [PubMed: 23281369]

71. Seneviratne U, Godoy LC, Wishnok JS, Wogan GN, and Tannenbaum SR (2013). Mechanism-based triarylphosphine-ester probes for capture of endogenous RSNOs. J. Am. Chem. Soc. 135, 7693–7704. 10.1021/ja401565w. [PubMed: 23614769]

72. van Ooijen MP, Jong VL, Eijkemans MJC, Heck AJR, Andeweg AC, Binai NA, and van den Ham HJ (2018). Identification of differentially expressed peptides in high-throughput proteomics data. Brief Bioinform. 19, 971–981. 10.1093/bib/bbx031. [PubMed: 28369175]

73. Mi H, Muruganujan A, Casagrande JT, and Thomas PD (2013). Large-scale gene function analysis with the PANTHER classification system. Nat. Protoc. 8, 1551–1566. 10.1038/nprot.2013.092. [PubMed: 23868073]

Highlights

- hiPSC-derived PD neurons manifest aberrantly S-nitrosylated TCA cycle proteins
- Human PD/LBD brains also manifest aberrantly S-nitrosylated TCA enzymes
- Metabolic flux experiments show SNO inhibition of the TCA cycle at αKGDH/SCS

SIGNIFICANCE

The present study links findings of compromised mitochondrial bioenergetics to TCA cycle compromise, precipitated by aberrant protein S-nitrosylation reactions on TCA cycle enzymes in PD and LBD brain. A central tenet in this work is that mutant genotype (G) in αSyn makes neurons more susceptible to environmental (E) influences, e.g., pesticides, which are known to be associated with PD/LBD, as shown previously in epidemiological studies and cell-based models using PD patient-derived hiPSCs. This gene by environment interaction, termed GxE, can be mediated via production of excessive RNS/NO, which is known to be synergistically enhanced by the presence of both an A53T mutation in αSyn and exposure to pesticides such as PQ/MB[5]. In the present study, we show how these elevated levels of NO affect metabolism via inhibition of the TCA cycle. From epidemiological studies in a real-world scenario, we know that both genotype and pesticides increase NO production contributing to nitrosative stress and PD risk. Hence, in the case of aberrantly S-nitrosylated (SNO)-proteins, genotype and pesticides work in concert as an example of GxE interaction. We show for the first time here a link between aberrant protein S-nitrosylation and TCA cycle enzyme inhibition to potentially contribute to PD/LBD pathogenesis.

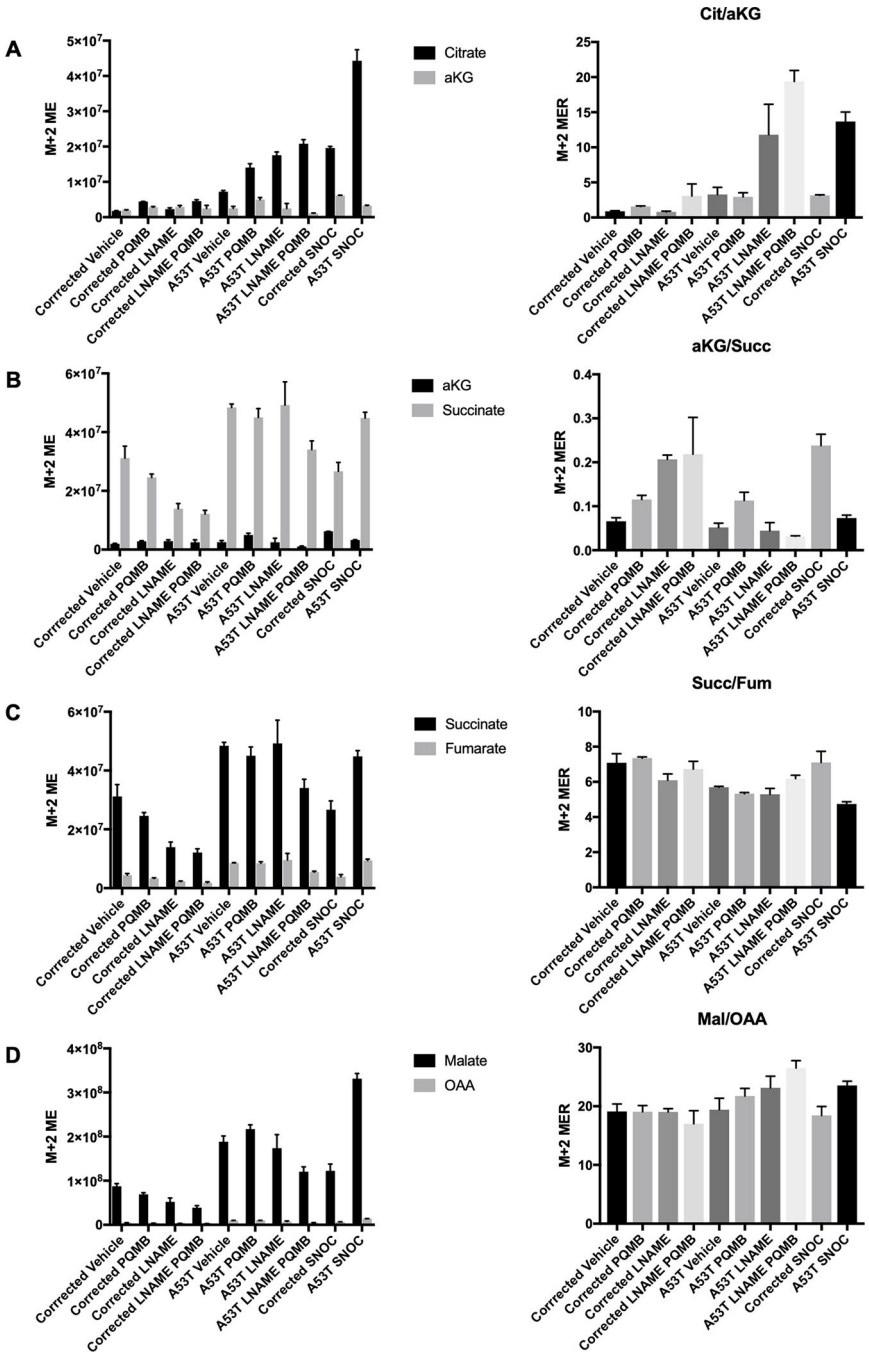

Figure 1. Metabolic flux analysis of TCA cycle enzymes

PD A53T-hiN vs. isogenic WT/Control hiN incubated with C^{13}-lactate. *Left-hand panels* show individual substrates and products; *right-hand panels* show ratio.

(A) Substrates and products for AC/ IDH enzyme reactions.

(B-D) Substrates and products for αKGDH enzyme reaction (panel B), for SDH (C), and for MDH (D). Values are mean + SEM, n ≥ 3 experiments. As seen in the A53T PD hiPSC-derived neurons exposed to PQ/MB, but not in isogenic gene-corrected controls, there is a block at the level of αKGDH which is reversed by L-NAME. Abbreviations:

cit, citrate; αKG, α-ketoglutarate; ME, molar percent enrichment; MER ratio of substrate/product molar enrichment; succ, succinate, fum, fumarate; mal, malate; OAA, oxaloacetate. Statistical significance, tested by ANOVA followed by a PLSD post hoc test,[62] is presented in the text. See also Figures S1–S3.

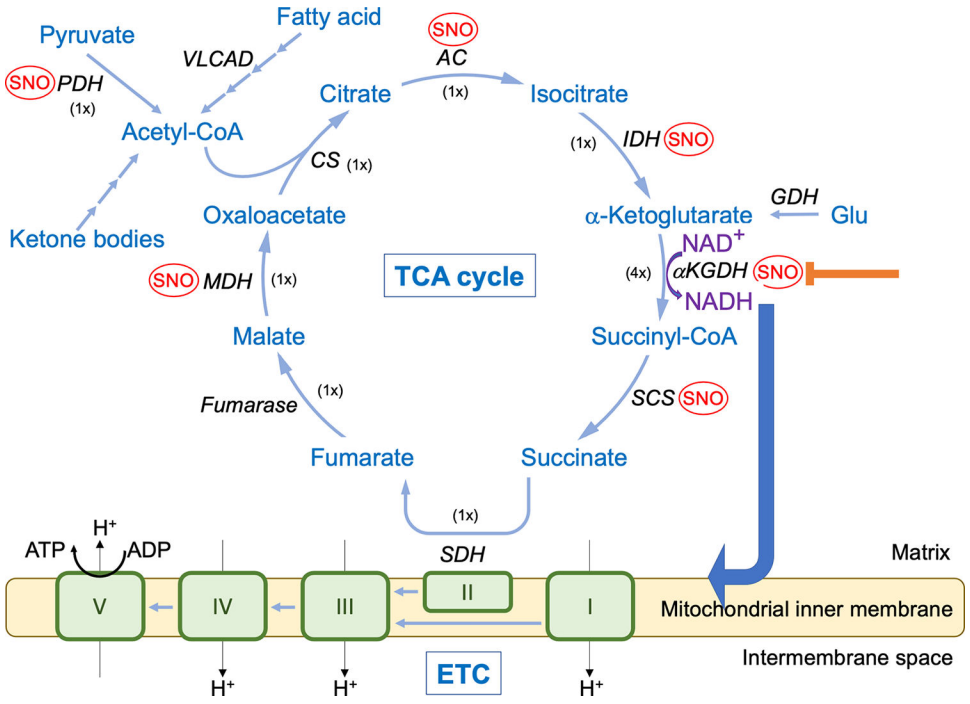

Figure 2. Schema showing effects of S-nitrosylation of TCA cycle enzymes in isogenic WT and A53T mutant αSYN hiN

A53T-hiN display basal partial inhibition of the TCA cycle at the AC/IDH steps. This is consistent with data that both of these enzymes are S-nitrosylated in A53T-hiN, particularly in the presence of PQ/MB. S-Nitrosylation of αKGDH results in more major enzyme inhibition, as evidenced by reversal by the NOS inhibitor L-NAME, and hence significant kinetic inhibition of flux through the TCA cycle at that point in the cycle. Note that the action of αKGDH also supplies NADH to the ETC for production of ATP. We have previously performed activity assays showing that S-nitrosylation of AC, IDH, αKGDH and other TCA enzymes can inhibit their activity.[11] At the level of MDH and PDH, which were also S-nitrosylated under A53T-PQ/MB conditions, a lesser degree of inhibition was observed. The fold difference in flux rate constants obtained by kinetic modeling (see Methods) in the absence and presence of L-NAME to show enzymes impacted by S-nitrosylation, is shown in parenthesis (with 4x representing a 4-fold increase and 1x representing no significant change).

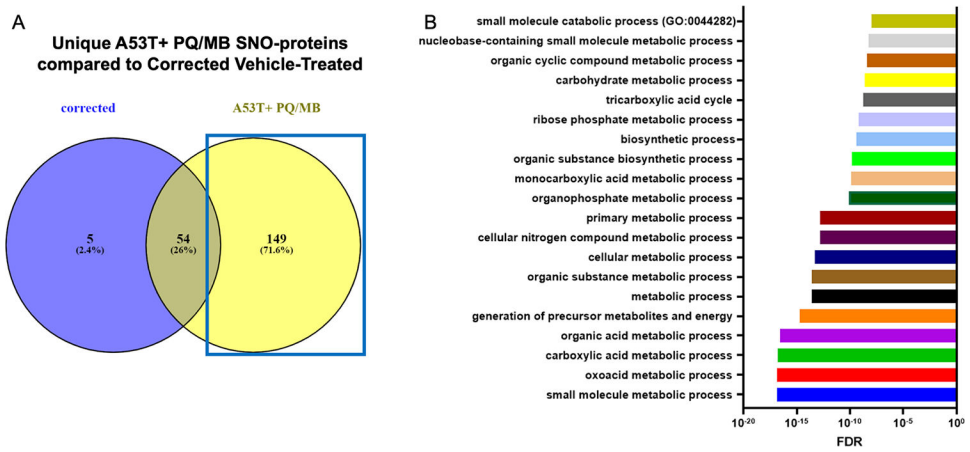

Figure 3. SNO-proteins found under PD conditions (A53T-PQ/MB) in hiN vs. corrected controls

(A) Venn diagram of SNO-proteins under A53T-PQ/MB conditions vs. corrected control. See also Table S1.

(B) GO-term analysis of the differences yielded these highest scoring pathways.

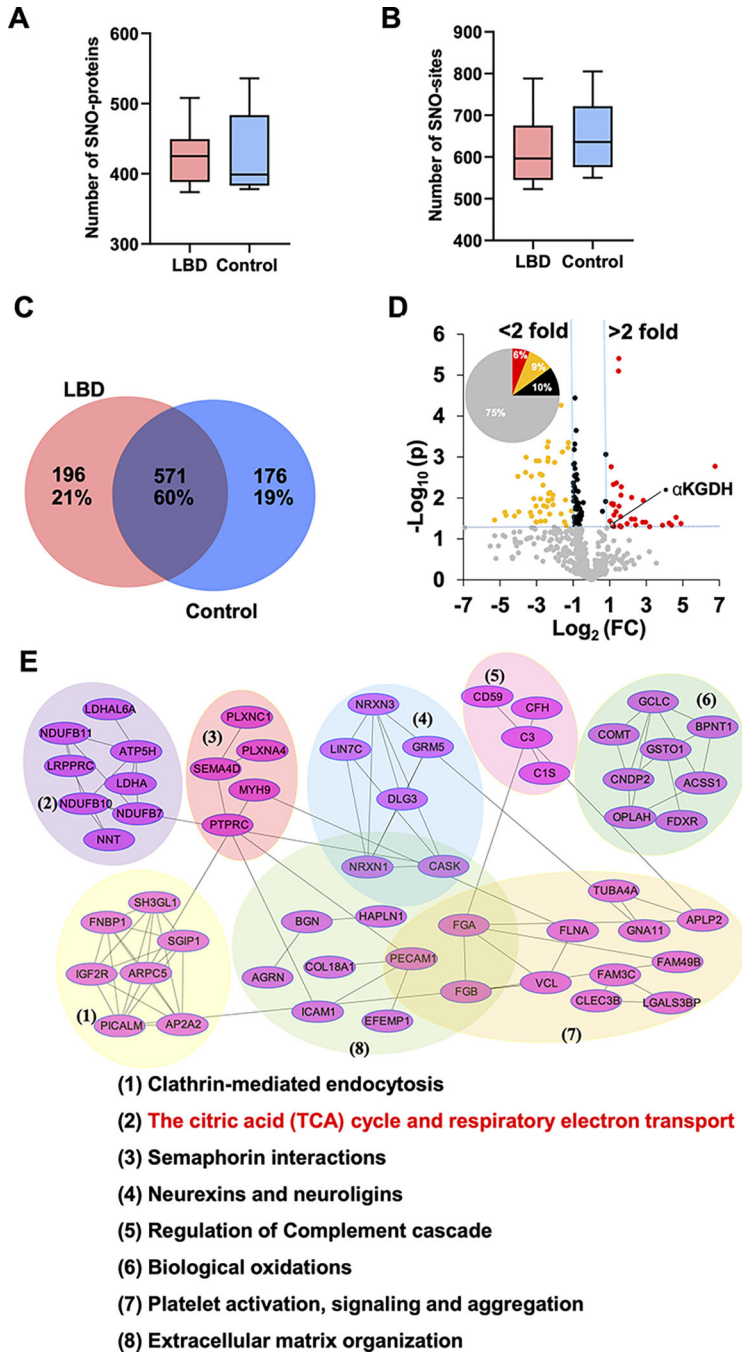

Figure 4. S-Nitrosoproteome and reactome analysis of affected pathways in LBD vs. control human brains

(A and **B)** Box and whisker plot of number of SNO-proteins (**A**) and SNO-sites (**B**) from each postmortem human brain (n = 6 LBD and 5 controls). Box-and-whiskers plots show the median, interquartile range, and minimum and maximum of SNO-proteins and SNO-peptides found per each group. See also Tables S2–S4.

(C) Venn diagram showing the number of SNO-proteins in LBD brains, control brains, and their overlap.

(D) Volcano plot showing distribution of upregulated and downregulated SNO-proteins in human LBD brain compared to controls. The predominantly upregulated TCA enzyme, SNO-αKGDH is indicated.

(E) Reactome analysis of pathways affected by aberrant protein S-nitrosylation in human LBD brains over controls. Data were analyzed with STRING software.

KEY RESOURCES TABLE

REAGENT or RESOURCE	SOURCE	IDENTIFIER
Antibodies		
Rabbit anti-Lipoamide dehydrogenase (DLD)	Abcam	Cat#ab133551; RRID:AB_2732908
Rabbit anti-Aconitase 2 (Aco2 or AC)	Cell Signaling Technologies	Cat#6922S; RRID:AB_10828218
Goat IRDye® 800CW anti-Rabbit IgG Secondary Antibody	LI-COR Biosciences	Cat#926-32211; RRID:AB_621843
Biological samples		
Human LBD and control brains	University of California (UCSD) Medical Center and the San Diego VA Medical Center Brain Bank	N/A
Chemicals, peptides, and recombinant proteins		
LDN-193189	REPROCELL Stemgent	Cat#04-0074-10
SB431542	Tocris Bioscience	Cat#1614
Recombinant Mouse Sonic Hedgehog/Shh (C25II)	R&D Systems	Cat#464-SH
Purmorphamine	REPROCELL Stemgent	Cat#04-0009
CHIR99021	REPROCELL Stemgent	Cat#04-0004-10
Recombinant Human/Murine/Rat BDNF	PeproTech	450-02
Recombinant Human GDNF	PeproTech	450-10
Recombinant Human TGF-beta 3 (TGFβ3)	Novus Biologicals	8420-B3-025
N^6,2′-O-Dibutyryladenosine 3′,5′-cyclic monophosphate sodium salt (dibutyryl cAMP or db-cAMP)	Millipore Sigma	Cat#D0627
DAPT	REPROCELL Stemgent	Cat#04-0041
Paraquat dichloride hydrate	Millipore Sigma	Cat#36541
Maneb	Millipore Sigma	Cat#45554
SODIUM ^{13}C-lactate	Cambridge Isotope Laboratories	CLM-1579-0.5
Nω-Nitro-L-arginine methyl ester hydrochloride (L-NAME)	Millipore Sigma	N5751
Organomercury resin	Doulias et al.[45]	N/A
S-methyl methanethiosulfonate (MMTS)	Millipore Sigma	Cat#208795
Biotin-HPDP(WS)	Dojindo Molecular Technologies	Cat#SB17
*SNO*TRAP	Seneviratne et al.[71]	N/A
Deposited data		
Proteomics data (human brains)	This paper	PXD036703
Proteomics data (hiPSCs)	This paper	PXD036797
Experimental models: Cell lines		
Human: A53T and gene-corrected, isogenic WT/Control hiPSCs	Soldner et al.[34]	N/A
Human: iCell DopaNeurons PD SNCA A53T	FUJIFILM Cellular Dynamics	Cat#C1113
Human: iCell DopaNeurons	FUJIFILM Cellular Dynamics	Cat#C1028

REAGENT or RESOURCE	SOURCE	IDENTIFIER
Software and algorithms		
Xcalibur	Thermo Fisher Scientific	N/A
Spectrum Mill MS proteomics Workbench	Agilent Technologies	N/A
MaxQuant	MaxQuant	N/A
Image Studio software	LI-COR Biosciences	N/A